A MECHANISTIC APPROACH TO CRYSTALLITE LENGTH AS RELATED TO CELL-WALL STRUCTURE[1]

M. Lotfy M. El-osta,[2] R. M. Kellogg, R. O. Foschi

Department of the Environment, Canadian Forestry Service
Western Forest Products Laboratory, Vancouver, British Columbia

and

R. G. Butters

Department of Metallurgy, University of British Columbia, Vancouver, B. C.

(Received 8 February 1974)

ABSTRACT

A tentative mechanistic model is proposed that relates variation in crystallite length in wood to some physical conditions under which the crystallite may have been formed, namely the curvature and ultrastructure of the microfibril. Over most of the experimental data range, representing both hardwood and softwood samples, the model allows reasonably good prediction of the effect of crystallite orientation angle and radial distance from the cell center. As the angle increases and radial distance decreases, the average crystallite length becomes smaller.

Additional keywords: Abies lasiocarpa, Tsuga heterophylla, Pseudotsuga menziesii, Populus tremuloides, Betula papyrifera, Acer macrophyllum, line-broadening, X-ray diffraction, cell diameter, degree of orientation, microfibril angle.

INTRODUCTION

There has been a growing interest in the study of interrelationships between ultrastructural features of wood cell walls and the basic physical properties of wood. Of particular interest have been studies concerned with effects of variation in microfibril angle. El-osta and Wellwood (1972) have found a strong inverse correlation between microfibril angle and crystallinity index. Furthermore, Marton et al. (1972) and Nomura and Yamada (1972) have reported an inverse relationship between crystallite length and microfibril angle. It was also indicated by Marton et al. that degree of crystallinity is correlated with crystallite length. However, to our knowledge no attempt has been made to offer an explanation for the observed relationship between crystallite length and microfibril

angle. It is the purpose of this paper to propose a tentative theory relating these factors in a causal way. We have expressed this theory with a mechanistic model that relates the crystallite length to some physical conditions under which that crystallite may have been developed.

The basic structural material of fiber or tracheid cell walls is cellulose. The manner in which cellulose-chain molecules form the basic framework units of cell walls during the complicated process of cell-wall formation is not well understood. Frey-Wyssling and Mühlethaler (1965) suggested that the development of fibrils is an end-growth phenomenon resulting from addition of glucose rings through polymerization and crystallization.

Research on cellulose has resulted in controversy on the size of the basic structural unit. This controversy may be due in part to the techniques used to separate and measure the units. Frey-Wyssling and Mühlethaler (1965), Heyn (1969), and Fengel (1970), to name a few, maintained that each microfibril contains linear bodies 3.5 nm wide called elementary fibrils. On

the other hand, Caulfield (1971), Bourret et al. (1972), and Nieduszynski and Preston (1970) support the existence of microfibrils having a diameter of 10–20 nm and containing a single crystalline core slightly smaller in size than the microfibril itself. However, it is generally agreed that the cellulose crystallites are surrounded laterally by cellulosic materials of lower degrees of order than the perfectly crystalline state (Preston 1971).

We make no pretence of contributing to the controversy on width and lateral order of microfibrils. It is not necessary for us to define the boundaries of the ultimate and absolute microfibril to express our theory. We choose to define the basic unit of our model as one containing a crystalline core surrounded laterally by a region of decreasing degree of order. The lateral limit of the basic unit is considered to be that region between units in which the degree of order is minimal. For ease in describing our theory, we have chosen to define our terms as follows. The perfectly crystalline region will be referred to as a crystallite or crystalline core, and the surrounding region of lesser degree of order, the amorphous shell. These two components will be defined as comprising a microfibril.

The model we propose envisions two major factors that might control crystallite length. The first of these is the curvature of the microfibril. The basic concept of the model is that there is a limited length of a linear body, i.e. a crystallite, which may be contained within a curvilinear body, i.e. the microfibril. An analogy to this concept is the limited length of straight rod that can be inserted into a curved tube. The second factor is the nature of the microfibril structure. In our model, the microfibril is described as having a single crystalline core surrounded by an amorphous shell. Whether the true microfibril has a single or multiple crystalline core structure is not critical to the concept. The essential parameters of this second factor are the relative diameters of the crystallite and surrounding amorphous shell, and the degree to which the surrounding material restrains the
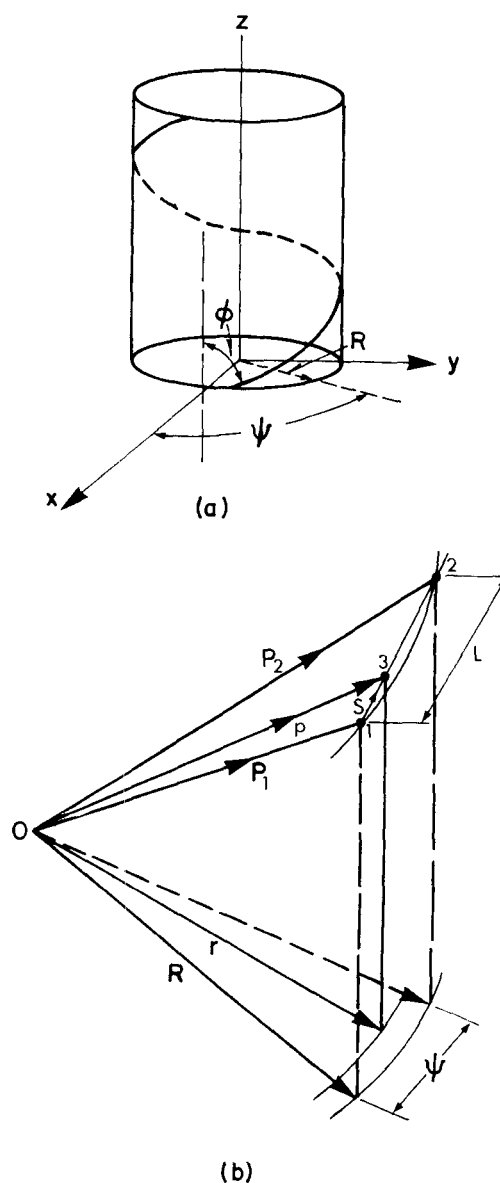

Fig. 1. Schematic representation of the model used for deriving the relationship between crystallite length (L) and crystallite orientation angle (ϕ). (a) represents a helix wrapped around a cylinder of radius R and (b) represents a straight segment (L) as controlled by its position in the structure.

lateral displacement of the crystallite within the larger microfibril body. If the amorphous shell in the developing microfibril is highly viscoelastic in nature, the crystalline

core might compress the surrounding shell and thus permit its extended linear development during formation. On the other hand, if the amorphous shell is rigid and incompressible, and if the microfibril has any degree of curvature, then the length of linear crystalline structure that could be accommodated within the microfibril is zero. In the aforementioned analogy, this is illustrated by the inability to insert a straight rod into a curved tube when the difference between the diameter of the rod and inside diameter of the tube is vanishingly small.

DEVELOPMENT OF THE THEORETICAL MODEL

We will now proceed to the development of the mathematical expression of this model. The cross-sectional shape of the fiber or tracheid in the model is considered to be cylindrical. Few longitudinal fibers or tracheids have this exact conformation, but the mathematics of a more realistic cell shape are extremely complex.

Consider the helix in Fig. 1a, wrapped around a cylinder of radius R. Consider also two points, 1 and 2 on the helix, and the straight segment 1–2 of length L (Fig. 1b). The vector to a generic point 3 along 1–2 is p, which has a horizontal projection r. Point 3 is at a distance S from point 1. The purpose is to find that value of S for which r is a minimum. It is simple to show that, for S = L/2, r has the minimum value given by:

$$r = R \cos \frac{\psi}{2} \quad . \qquad (1)$$

Thus, R and r = R cos ($\psi/2$) determine two concentric circular cylindrical surfaces within which the segment of length L is contained touching the outside surface at points 1 and 2 and touching the inside surface at point 3 for S = L/2. For a given pair of radii, r and R, L is the longest straight segment that can be accommodated between both surfaces.

Let us relate the length (L) of 1–2 to the angle ψ. If n_x, n_y and n_z are unit vectors

parallel to the x, y, and z directions respectively, ψ is the azimuthal angle and ϕ is the helix angle, the vector $\vec{1\text{-}2}$ can be expressed as (Fig. 1b):

$$\vec{1\text{-}2} = \vec{P}_2 - \vec{P}_1$$
$$= (R \cos \psi - R) \, \vec{n}_x$$
$$+ R \sin \psi \, \vec{n}_y + \frac{R \psi}{\tan \phi} \, \vec{n}_z \quad . \qquad (2)$$

Therefore:

$$L^2 = R^2 \cos^2 \psi - 2R^2 \cos \psi$$
$$+ R^2 + R^2 \sin^2 \psi + \frac{R^2 \psi^2}{\tan^2 \phi}$$
$$= 4R^2 \left[(1 - \cos^2 \frac{\psi}{2}) + \frac{\psi^2}{4 \tan^2 \phi} \right] . \qquad (3)$$

Introducing r/R from equation (1) into (3):

$$L_{max} = 2R \sqrt{1 - \left(\frac{r}{R}\right)^2 + \frac{1}{\tan^2 \phi} \left[\cos^{-1}\left(\frac{r}{R}\right)\right]^2} \quad . \qquad (4)$$

Equation (4) gives the maximum length of the straight element contained between two cylindrical surfaces, one of radius r and the other of radius R (where r < R), with the condition that the ends of the element are on a helix of an angle ϕ and on a surface of radius R.

Consider a crystallite having a diameter d (Fig. 2). Its center can be located in the microfibril at most at $R = R_0 + D\text{-}c\text{-}d/2$ from the cell center and as close to it as $r = R_0 + c + d/2$, where c is some distance, the nature of which is discussed below, D is the microfibril diameter, d is the crystallite diameter and R_0 is the radius to the inside of the microfibril. In other words, we assume that the crystallite centers form straight lines with ends on a helix located on a cylindrical surface R and the crystallites can be contained between two surfaces with radii r and R.

$$\therefore \quad \frac{r}{R} = \frac{1}{1 + \dfrac{D - d - 2c}{R_0 + c + d/2}} \quad . \qquad (5)$$

Since the radius R_0 is much larger than

$\mathfrak{C}$ Cell

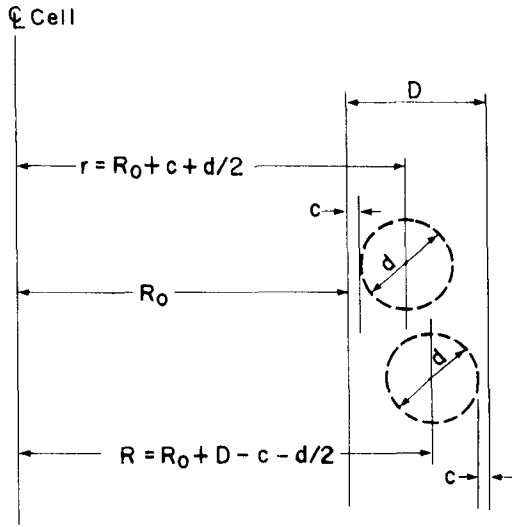

Fig. 2. Position of a crystallite of a diameter (d) within a microfibril relative to a cell center.

either D, d or c, r/R can be approximated as follows:

$$\frac{r}{R} \approx 1 - \frac{D - (d + 2c)}{R_0} \qquad (6)$$

Letting $\cos^{-1}(r/R) = w$, and r/R being close to 1,

$$\therefore \ \frac{r}{R} = \cos w \approx 1 - \frac{w^2}{2} \ ,$$

$$\therefore \ \left[\cos^{-1}\left(\frac{r}{R}\right)\right]^2 = w^2 \approx 2\left(1 - \frac{r}{R}\right) \ . \qquad (7)$$

Furthermore,

$$1 - \left(\frac{r}{R}\right)^2 = \left(1 + \frac{r}{R}\right)\left(1 - \frac{r}{R}\right) \ ,$$

$$\therefore \ 1 - \left(\frac{r}{R}\right)^2 \approx 2\left(1 - \frac{r}{R}\right) \ . \qquad (8)$$

Considering Eqs. (7) and (8), Eq. (4) becomes:

$$L_{max} = \sqrt{8R_0^2 \left(1 - \frac{r}{R}\right)\left[1 + \frac{1}{\tan^2 \phi}\right]} \ . \qquad (9)$$

Substituting (6) into (9):

$$L_{max} \approx \frac{\alpha \sqrt{R_0}}{\sin \phi} \ , \qquad (10)$$

where

$$\alpha = \sqrt{8(D - d - 2c)} \ . \qquad (11)$$

Equation (10) gives the approximate maximum length of cellulose crystallites as estimated by the model. The constant α cannot be measured directly, but it can be obtained by fitting Eq. (10) to experimental data. The model can then be confirmed by how well Eq. (10) fits the data.

A tentative physical interpretation may be given to the constant α. If the thickness of the amorphous shell is e = (D–d)/2 and the crystallite core compresses the shell to a thickness c, the percentage compressibility (γ) is defined as

$$\gamma = \frac{e - c}{e} \times 100 \qquad (12)$$

from which

$$D - d - 2c = \frac{2 \gamma e}{100} \qquad (13)$$

Therefore, introducing Eq. (13) into Eq. (11),

$$\alpha = 0.4 \sqrt{\gamma e} \qquad (14)$$

and thus, in Eq. (10),

$$L_{max} \approx \frac{Q}{\sin \phi} \qquad (15)$$

where:

$$Q = 0.4 \sqrt{R_0 \gamma e} \ . \qquad (16)$$

EXPERIMENTAL

To examine the proposed theory, test specimens were prepared from eight different samples representing three softwood and three hardwood species. This material permitted an experimental evaluation of the effect on crystallite length of variations in crystallite orientation angle (ϕ) and radial position (R_0), since a wide range of ϕ can be obtained by test specimen preparation and the species selected exhibited a variation in fiber or tracheid diameters.

Specimen preparation

Wood samples (nominal 2 cm radially, 1 cm tangentially, and 8 cm longitudinally) of alpine fir [*Abies lasiocarpa* (Hook.) Nutt.], western hemlock [*Tsuga heterophylla* (Raf.) Sarg.], trembling aspen (*Populus tremuloides* Michx.), white birch

(*Betula papyrifera* Marsh.) and bigleaf maple (*Acer macrophyllum* Pursh.) and two compression-wood samples of Douglas-fir [*Pseudotsuga menziesii* (Mirb.) Franco] were machined from available stock at the Western Forest Products Laboratory. Each sample contained a number of narrow growth increments and was free of defects.

Using a micro-saw (Bramhall and McLauchlan 1970), 10 end-matched cross sections (nominal 2 cm radially, 1 cm tangentially, and 3 to 4 mm longitudinally) were machined from each sample. The first specimen of each series was cut from the radial-tangential plane and was, therefore, a true cross section. The other specimens of each series were sawn such that the normal to their surfaces deviated from the longitudinal direction by a rotation about the radial axis of 5 to 45° in 5° increments (Fig. 3).

Estimates of crystallite length based on the (040) reflection result from crystallites oriented in the direction of the diffraction vector, i.e. normal to the specimen surface. The series of specimens thus prepared provided estimates of crystallite length for crystallites in the tangential walls, with the corresponding range of orientation from the fiber or tracheid axis.

At small crystallite orientation angles, diffraction arises from crystallites in the radial walls as well. However, as ϕ increases, diffraction from the radial walls arises only from crystallites that exhibit angular deviation out of the plane of the cell wall.
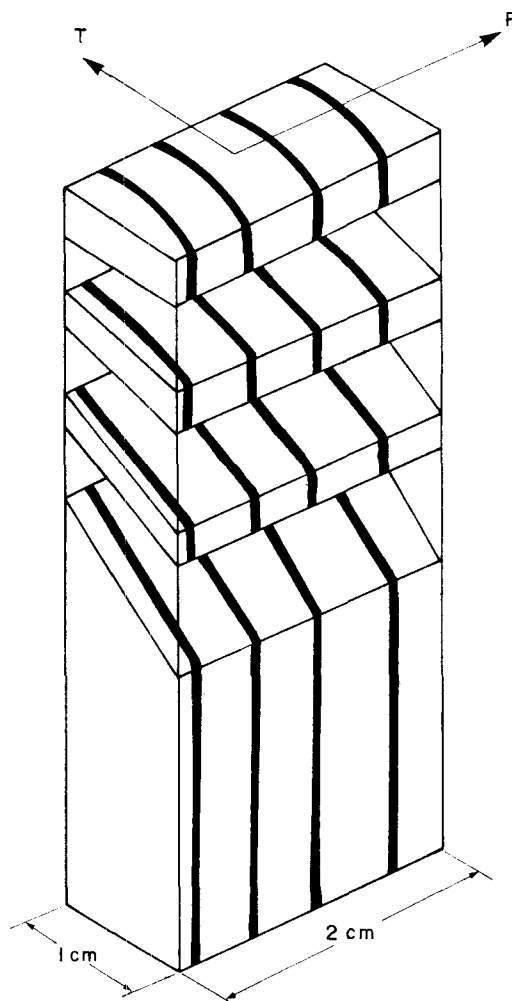

Fig. 3. Schematic diagram showing the preparation of experimental specimens. R and T designate the radial and tangential directions, respectively.

Scanning the (040) reflection

A Philips goniometer PW 1050 and X-ray generator PW 1011 were used for scanning the (040) reflection. Nickel-filtered copper X-radiation was employed and 1° divergent and receiving slits were used in the goniometer. The diffraction profile was recorded in steps of 0.05° (2θ) from 30° to 38° (2θ), using a fixed-time counting technique (40 seconds). A proportional counter, pulse-height analyzer, scaler, and printer were utilized.

Numerical analysis for resolving the (040) reflection

The (040) reflection ($2\theta \simeq 34.5°$ for Cu Kα) of cellulose I is unfortunately contaminated by reflections arising from other planes. These planes and their corresponding (2θ) angles (Cu Kα) that give rise to the above-noted interference (Mann et al. 1960) are listed in Table 1.

Fortunately, the contaminating reflections are much weaker than (040) itself.

TABLE 1. *List of planes and their corresponding (2θ) angles contaminating the (040) reflection (2θ ≃ 34.5° for Cu Kα) of cellulose I*

hkl	(2θ)	hkl	(2θ)
131 $\overline{1}$31	30.6	310 212 311 013 113	34.3
$\overline{2}$21 $\overline{1}$22	31.5		
300 202 301 003 103	33.5	140 041	36.2
230 032	34.1	231 132 $\overline{2}$31 132 232	36.4

Since their presence does affect the profile of the reflection under consideration, a numerical analysis was devised to resolve the (040) reflection from the composite profile and to calculate its breadth at half of maximum peak intensity.

For the purpose of conducting the numerical analysis, a computer program[3] was written. The program considers that the observed X-ray intensity distribution is composed of intensity contributions from each of the eight reflections mentioned above superimposed upon a background intensity (I_B). The latter was expressed by the following cubic polynomial:

$$I_B(m) = A_1^2 + A_2 (m-m_0) + A_3 (m-m_0)^2 + A_4 (m-m_0)^3 \qquad (17)$$

where: A_1 through A_4 = unknown constants,
m = (2θ) angle and
m_0 = a reference (2θ) angle that can be taken as that of the first observation.

Each of the eight overlapping peaks was considered to have a Gaussian shape represented as follows:

$$I_n(m) = A_{2n+3}^2 \ EXP \left[-A_{2n+4}^2 \ (m-v_n)^2 \right] \qquad (18)$$

---

[3] The program is available from the Western Forest Products Laboratory, 6620 N.W. Marine Drive, Vancouver, B.C., V6T 1X2.

where: n = 1, 2 .... 8 and
v = the (2θ) angle at which the peak occurs.

In the above equation A_{2n+3} is the peak intensity, whereas A_{2n+4} is related to its breadth (B_n) at half height in the following manner:

$$A_{2n+4} = \frac{\sqrt{4 \ \cdots \ 2.0}}{B_n} \ . \qquad (19)$$

The total observed X-ray intensity was therefore represented by the following expression:

$$I(m) = A_1^2 + A_2 \ (m-m_0)$$
$$+ A_3 \ (m-m_0)^2 + A_4 \ (m-m_0)^3$$
$$+ \sum_{n=1}^{8} A_{2n+3}^2 \ EXP \left[-A_{2n+4}^2 (m-v_n)^2 \right]. \qquad (20)$$

The twenty unknown constants were determined by the least-squares fit of Eq. (20) to the X-ray intensities from 30° to 38° (2θ). Thus, if $I_D(m_i)$ is the observed intensity at m_i angle and $I(m_i)$ is the intensity given by Eq. (20) for the same angle, the condition that

$$J = \sum_{i=1}^{NP} \left[I_D(m_i) - I \ (m_i) \right]^2 \qquad (21)$$

where: NP = number of data points

be a minimum allowed the determination of the unknown constants in Eq. (20). The minimization of J was achieved by using Fletcher and Powell's method (1963). After determining the "A" constants, Eqs. (19) and (20) allowed direct calculations of the resolved (040) peak intensity as well as the breadth at half of its height.

Crystallite length determination

Crystallite length was obtained from the line profile for the resolved (040) reflection by applying the following Sherrer equation (Klug and Alexander 1954):

D = Kλ/β cos θ,

where: D = average crystallite size normal to diffracting planes,
K = constant (0.9),
λ = X-ray wave length (0.1542 nm),

TABLE 2. *Average crystallite length* (*nm*) *as a function of their angle to the tracheid or fiber axis*

Species	Angle to tracheid or fiber axis (degrees)									
	0	5	10	15	20	25	30	35	40	45
Softwoods										
Alpine fir	31.1	23.3	22.6	21.3	20.0	12.9	9.1	4.5	4.1	4.3
Douglas-fir compression wood #1	31.1	22.6	26.0	20.0	21.8	12.9	8.9	6.6	5.0	4.5
Douglas-fir compression wood #2	28.2	25.1	24.2	22.6	17.2	17.2	11.5	8.4	4.7	-
Western hemlock #1	28.2	25.1	-	24.2	18.5	16.5	11.2	7.2	5.9	4.9
Western hemlock #2	24.2	28.2	28.2	25.1	23.3	17.6	10.8	5.0	5.1	4.2
Hardwoods										
Aspen, trembling	28.2	25.1	21.8	19.0	15.4	11.9	9.5	5.7	5.1	4.2
Birch, white	26.0	26.0	21.8	18.1	17.6	11.5	7.0	5.0	4.2	4.6
Maple, bigleaf	22.6	23.3	16.8	16.1	9.6	4.9	4.7	5.1	5.0	4.5

θ = Bragg's angle (17.25°) and
β = the pure breadth for the (040) at half-peak intensity (in radians).

The observed line breadth at half-peak intensity (B) for the (040) reflection is due to the combined effects of average crystallite strain, and instrumental broadening (Klug and Alexander 1954). Accordingly, in order to apply Sherrer's equation, it was assumed that no strains were present, and the observed line breadth was corrected for instrumental line broadening. Hexamethylenetetramine $(CH_2)_6N_4$ was used as a standard for assessing the instrumental line broadening under identical experimental conditions. This standard has been used by Shenouda and Viswanathan (1972) and Viswanathan and Venkatakrishnan (1969). For $(CH_2)_6N_4$ crystals, the instrumental line broadening (b) amounted to 0.24° (2θ). Warren's correction (Klug and Alexander 1954) was applied for calculating β in Sherrer's equation whereby $\beta = (B^2 - b^2)^{1/2}$.

Estimates of R_o for the experimental material could not be determined with precision because the exact position of the diffracting crystallites within the cell walls cannot be ascertained. However, on the basis of the known microfibril orientation within the cell-wall layers, it might be expected that for crystallite angles ranging from 0° to 45°, most of the diffraction would arise from crystallites within the S_2 layer. It was decided that an approximate measure of R_o could be taken as slightly less than half of the average tracheid or fiber diameter to account for wall thickness. These diameter measurements were made on cross-sectional microtome slides prepared from each sample. The average diameter was estimated with the aid of a projecting microscope from cell counts within a known width of measuring field. For each sample, the average diameter was determined from 20 sets of cell counts.

RESULTS AND DISCUSSION

Calculated crystallite lengths and the corresponding angles the crystallites make with the tracheid or fiber axis for different species are presented in Table 2. The crystallite length values may be slightly underestimated because of the fact that part of the measured line broadening is due to crystalline strain. Correction for this effect cannot be made.

The basic data for the relationship between crystallite orientation angle (ϕ) and crystallite length (L) are shown in Table 2 and plotted in Fig. 4 for all eight samples. A similar pattern of decreasing crystallite length with increasing crystallite orientation angle is evident for all samples.

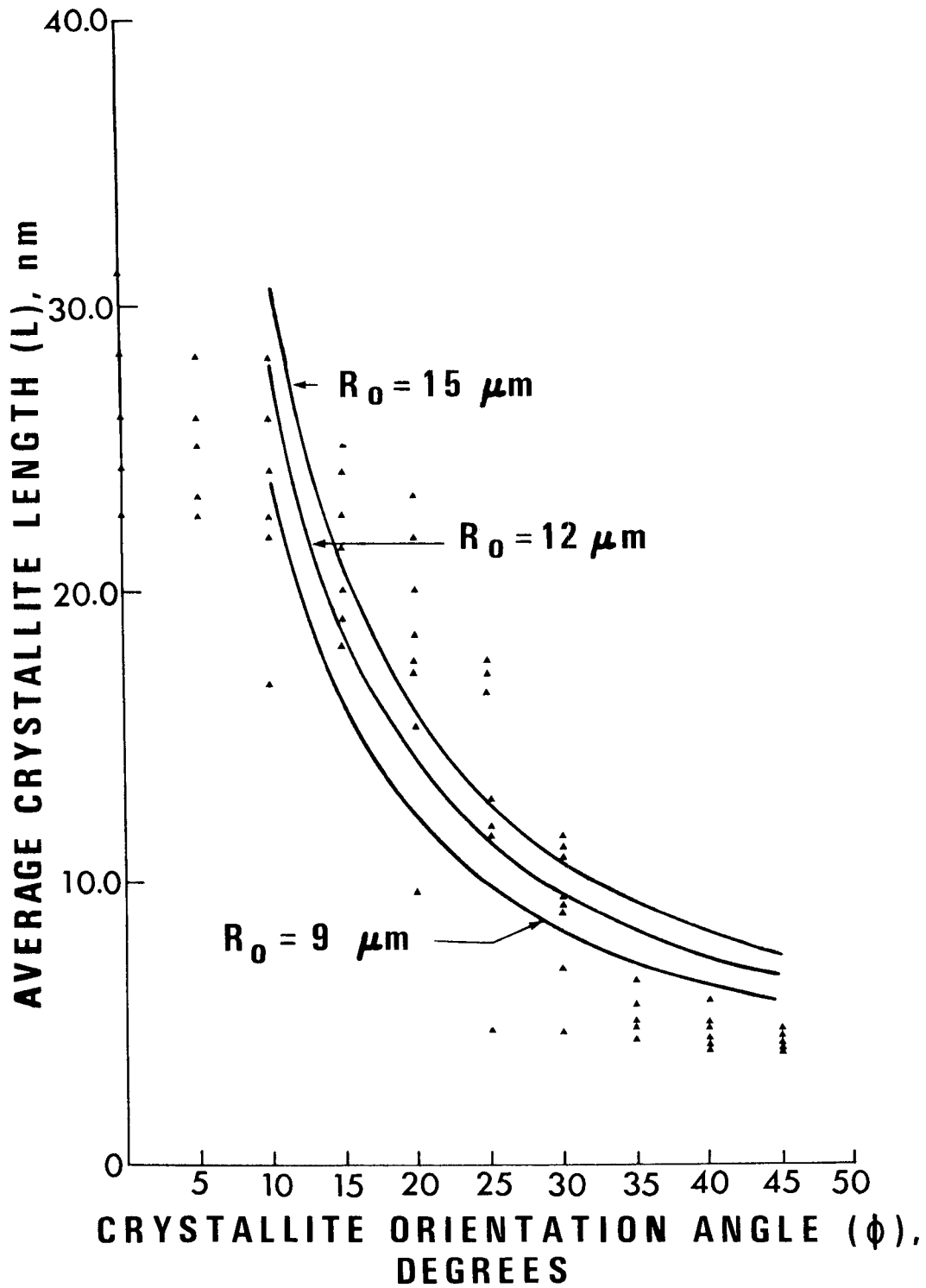Equation (10) was fitted to the experi-

FIG. 4. Experimental data for crystallite length (L) as a function of crystallite orientation angle (ϕ) and the theoretical relationship between L and ϕ as a function of R_0

mental data. The value of R_0 was taken as 12μm, a reasonable average for these species. The value of α obtained was $\alpha = 0.04382$ and the regression curve is plotted in Fig. 4. The general shape of the predicted curve fits the data quite well over its mid-range. The curve reaches an asymptote of 4.8 nm at $\phi = 90°$. It appears that the experimental data reach this same level, but at a lower value of crystallite orientation angle. At $\phi = 0°$, the model goes to infinity. Obviously this is an impossibility, for the fiber or the tracheid itself has finite length. The experimental data deviate markedly from the predicted curve at crystallite orientation angles of less than 10°. Perhaps the microfibrils weave slightly within the wall as they appear to do in many electron micrographs so that, even with an average orientation of 0°, curvature is present and the crystallite length thereby is limited.

The estimate of amorphous shell thickness (e) is taken as 0.6 nm based on the estimate of average distance between crystallites of 1.2 nm (Berlyn 1970). Using $\alpha = 0.04382$ and Eq. (14), the value of γ, the percentage compressibility of the amorphous shell, is found to be $\gamma = 0.02\%$. If the interpretation of α given by Eq. (14) is physically valid, the value obtained for γ means that the amorphous shell is laterally compressed only minutely before the crystallite is disrupted in its linear development.

It must be realized that the experimental data were obtained on air-dry specimens only. Whether or not removal of water could have affected the average crystallite length remains to be seen. In addition, the model was developed for cells of circular cross section; nevertheless this does not invalidate the application of the concept to noncircular cells. A cell approaching a rectangular shape will have portions of its wall with both greater and lesser curvature than that for a circular cell of the same average diameter. Thus, the range of maximum crystallite lengths would be increased for a given crystallite orientation angle, but the average value obtained from the diffractions from a large number of cells might

Table 3. *A comparison between $Q(i.e., 0.4\sqrt{R_o}\gamma e)$ and Q_1 (i.e., regression coefficient)*

	Cell diameter (μm)	Q (nm)	Q_1 (nm)
Softwoods			
Alpine fir	33	5.63	4.61
Douglas-fir compression wood #1	34	5.71	4.95
Douglas-fir compression wood #2	29	5.28	5.06
Western hemlock #1	34	5.71	5.86
Western hemlock #2	30	5.37	5.61
Hardwoods			
Aspen, trembling	26	5.00	4.27
Birch, white	25	4.90	4.20
Maple, bigleaf	22	4.60	3.13

be very similar to that obtained for more circular cells. The weaving patterns of microfibrils would be a limiting factor for crystallite length even for flat-sided cells.

Interest was next directed to determining whether the variation in the crystallite length-crystallite orientation angle relationship between species is related to their differences in cell diameter, which would directly affect the values of R_0 in the model. The average diameters of tracheids or fibers for the samples are listed in Table 3. From this information, the average cell radius was taken as an estimate of R_0 for each species. Substituting these values of R_0 and fixed values of $\gamma = 0.02\%$ and $e = 0.6$ nm into Eq. (16) yielded a constant Q for each species. A regression analysis of the L vs. ϕ data, excluding the data points for $\phi = 0°$ and $5°$, and using the function $Q_1/\sin\phi$ was conducted for each species. The values of Q and Q_1 so derived are shown in Table 3.

A rank correlation indicated that the association between Q and Q_1 is significant at the 1% level. This substantiates that part of the variability in the crystallite length at a fixed ϕ angle is due to the variation in cell diameter.

To check the present model further as a function of R_0, Eq. (10) was used to derive the theoretical relationship between L and

ϕ for $R_0 = 15$ μm and $R_0 = 9\mu$m. These relationships are also plotted in Fig. 4. Examination of these relationships indicates that the model is sensitive to R_0 and that the predicted variation in L resulting from the change in R_0 assigned to our material is reasonably similar to that determined experimentally.

The test of the theoretical model for crystallite length that we have proposed is not rigorous, namely because of our inability to measure the parameters included in the constant, a. We feel, however, that the concept is reasonable and supported sufficiently by the experimental results to offer it as a working model worthy of further experimental investigation.

SUMMARY AND CONCLUSION

A theory relating crystallite length with the physical conditions under which the crystallite may have been developed is presented in the form of a mechanistic model. The model considers two basic factors. The first of these is the curvature of the microfibril as determined by the microfibril orientation and the radial distance from the cell center. The second factor has been expressed by a constant that may be related to certain cross-sectional properties of the microfibril.

On the basis of measurements made on both hardwood and softwood samples, the influence of the above-mentioned microfibrillar curvature factors on crystallite length appears to be predicted reasonably well by the theoretical model presented. Crystallite lengths for the experimental material varied from 4.2 nm to 31.1 nm, decreasing with increasing crystallite orientation angle and decreasing radial position.

REFERENCES

BERLYN, G. P. 1970. Ultrastructural and molecular concepts of cell-wall formation. Wood Fiber 2(3):196–227.

BOURRET, A., H. CHANZY, AND R. LAZARO. 1972. Crystallite features of Valonia cellulose by electron diffraction and dark field electron microscopy. Biopolymers 11(4):893–898.

BRAMHALL, G., AND T. A. McLAUCHLAN. 1970. The preparation of microsections by sawing. Wood Fiber 2(1):67–69.

CAULFIELD, D. F. 1971. Crystallite sizes in wet and dry Valonia ventricosa. Text. Res. J. 41:267–269.

EL-OSTA, M. L. M., AND R. W. WELLWOOD. 1972. Short-term creep as related to cell-wall crystallinity. Wood Fiber 4(3):204–211.

FENGEL, D. 1970. Ultrastructural behavior of cell-wall polysaccharides. Tappi 53(3):497–503.

FLETCHER, R., AND M. POWELL. 1963. A rapidly convergent descent method for minimization. Comput. J. 6:163–168 (FMFP routine in IBM's Scientific Package).

FREY-WYSSLING, A., AND K. MÜHLETHALER. 1965. Ultrastructural plant cytology. Elsevier, New York. Pp. 34–40.

HEYN, A. N. J. 1969. The elementary fibril and supermolecular structure of cellulose in softwood fiber. Pages 27–49 in D. H. Page, ed. The physics and chemistry of wood pulp fibers. Tappi Stap Ser. No. 8.

KLUG, H. P., AND L. E. ALEXANDER. 1954. X-ray diffraction procedure. Wiley, New York. Pp. 491–538.

MANN, L., L. ROLDAN-GONZALEZ, AND H. J. WELLARD. 1960. Crystallite modification of cellulose. Part IV. Determination of X-ray intensity data. J. Polymer Sci. 42:165–171.

MARTON, R., P. RUSHTON, J. S. SACCO, AND K. SUMIYA. 1972. Dimensions and ultrastructure in growing fibers. Tappi 55(10):1499–1504.

NIEDUSZYNSKI, I., AND R. D. PRESTON. 1970. Crystallite size in natural cellulose. Nature 225:273–274.

NOMURA, T., AND T. YAMADA. 1972. Structural observation on wood and bamboo by X-ray. Wood Res. (Japan) 52:1–12.

PRESTON, R. D. 1971. Negative staining and cellulose microfibril size. J. Microsc. 93:7–13.

SHENOUDA, S. G., AND A. VISWANATHAN. 1972. Crystalline character of native and chemically treated Egyptian cottons. II. Computation of variance of X-ray line profile and paracrystalline lattice distortions. J. Appl. Polymer Sci. 16:395–406.

VISWANATHAN, A., AND V. VENKATAKRISHNAN. 1969. Disorder in cellulosic fibers. J. Appl. Polymer Sci. 13:785–795.